Geostrophic Scatter Diagrams and Potential Vorticity Dynamics

P. L. READ

Meteorological Office, London Road, Bracknell RG12 2SZ, U.K.

P. B. RHINES

School of Oceanography, University of Washington, Seattle, WA 98195

A. A. WHITE

Meteorological Office, London Road, Bracknell RG12 2SZ, U.K.

(Manuscript received 3 February 1986, in final form 11 August 1986)

ABSTRACT

A scatter diagram may be constructed by choosing an appropriate closed or open horizontal curve in physical space and plotting the value of any scalar quantity q against the geostrophic streamfunction ψ for each data point on the curve. The area enclosed on the scatter diagram is equal to the net geostrophic advective flux of q across the chosen curve in physical space. When q is the (quasi-geostrophic) potential vorticity Q, and suitable normalizations are adopted, this result may be exploited to derive measures of departure from free-mode form $Q = Q(\psi)$ along the curve in physical space. For a certain class of open space curves, an appropriate measure is the width-to-length ratio of the circuit in (ψ, Q) space. Most scatter diagrams that have appeared in the literature included the (ψ, Q) points corresponding to all the data or grid points within a given horizontal domain. The significance of the area enclosed on these diagrams is less clear, but the spread about some curve $Q = Q(\psi)$ is evidently a qualitative measure of the extent to which the flow deviates from free-mode form. For steady or time-averaged flows which are approximately of this form, the gradient $dQ/d\psi$ of the scatter diagram may be used to infer some properties of the forcing and dissipative processes acting. When dissipation is principally due to Q-transfer by transient eddy motion (or viscosity), the key diagnostic relation is

$$\frac{dQ}{d\psi} = -\frac{\iint S dx dy}{K \int \mathbf{v} \cdot d\mathbf{l}}$$

where S is the potential vorticity forcing, K the lateral eddy (or viscous) diffusivity, $\mathbf{v}$ the horizontal velocity, and the integrals are taken over and around any region enclosed by a mean streamline. Hence $dQ/d\psi$ is often negative, corresponding to two common properties of quasi-geostrophic circulations: that the eddy motion (or viscosity) transport Q down its mean gradient ($K > 0$) and that the circulation integral have the same sign as the potential vorticity forcing. Two sets of examples, both involving (Q, ψ) scatter diagrams constructed from numerically simulated data, are presented. One relates to steady baroclinic wave motion in a rotating annulus system, and the other to the time-averaged circulation in an ocean basin.

1. Introduction

It is well known that examination of the potential vorticity field can provide useful insight into the dynamics of rotating geophysical flows—as regards both general circulations and individual motion systems, and in observational, numerical and theoretical contexts. Thus, the quasi-geostrophic potential vorticity (Q) field is known to be central to the dynamics of time-varying flows, in which the time average and perturbation fields interact to produce Rossby waves, flow instability, wave–mean flow interaction and the turbulent cascade which carries potential vorticity to small scales. Flows in which Q is functionally related to the geostrophic streamfunction ψ appear as important special cases. Such "free mode" configurations can emerge from random initial conditions (e.g., see Bretherton and Haidvogel, 1976; Rhines, 1977; McWilliams, 1984), and they also characterize the ideal fluid (nondiffusive, steady state) description of large-scale ocean circulation—provided that the effects of mesoscale eddies are small or are balanced by other agencies. When the functional relation $Q = Q(\psi)$ is linear, free modes are susceptible to analytical treatment; thus modons (see Stern, 1975; Flierl et al., 1980; Tribbia, 1984) and finite amplitude Rossby waves (see Kuo, 1959; Mitchell and Derome, 1983; Derome, 1984; Read, 1985; White, 1986) are solutions of this type when viewed in an appropriate coordinate frame.

Several recent papers on quasi-stationary geophysical

flows have included "scatter diagrams" in which the values of Q calculated at many locations are plotted against the corresponding values of ψ. Examples using numerical model data appear in Bretherton and Haidvogel (1976), McWilliams and Zabusky (1982), McWilliams (1983), and Shutts (1983), while Illari and Marshall (1983) plot initialized atmospheric data.

In such diagrams the spread of the points about some (single-valued) curve $Q = Q(\psi)$ is clearly of interest, for if the points collapse precisely onto such a curve then the flow pattern is of free mode form. Although it is clear that the greater the spread of points about $Q = Q(\psi)$ then the more does the flow deviate from free mode form, no quantitative interpretation of the spread has—to our knowledge—been given. In this paper we point out a simple physical interpretation of scatter diagrams obtained by plotting the values of Q and ψ that correspond to certain curves in physical (x, y) space. The essential result to be derived applies to any scalar quantity q, and this general case will be treated first in section 2. Examples in which q is a suitably defined potential vorticity are given in sections 3 and 4.

When the points on a (Q, ψ) scatter diagram do not deviate greatly from some smooth curve $Q = Q(\psi)$, the slope $dQ/d\psi$ can be used to determine certain characteristics of the forcing and dissipative processes acting on the flow. We develop in section 4 a simple framework (based on the work of Rhines and Young (1982, 1983); see also Pierrehumbert and Malguzzi, 1984; and Marshall and Nurser, 1986) for relating the potential vorticity source to $dQ/d\psi$ and the circulation around a closed streamline. Some concluding remarks are offered in section 5.

2. Curves in physical and (ψ, q) space

Figure 1a shows a simple closed circuit ABCDA in physical (x, y) space, and contours of an imagined geostrophic streamfunction (ψ) field. The points A and C

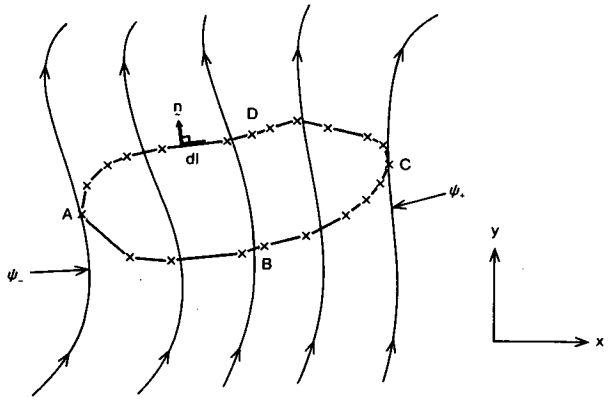

FIG. 1a. A closed circuit ABCDA in the (x, y) plane and contours of a geostrophic streamfunction ψ.

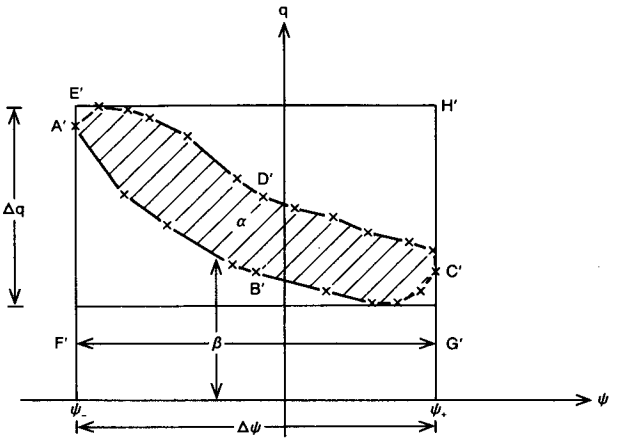

FIG. 1b. A circuit A'B'C'D'A' in the (ψ, q) plane which corresponds to the circuit ABCDA in the (x, y) plane. See text for further details.

are chosen to be lowest (ψ_-) and highest (ψ_+) streamfunction values on the circuit; B and D merely allow easy identification of the sense in which the circuit is traversed; arrows indicate the direction of the geostrophic flow $\mathbf{v}_g$ ($=\mathbf{k} \times \nabla\psi$, where $\mathbf{k}$ is unit vertical vector) and crosses indicate notional data points on the circuit. The shape of ABCDA is arbitrary except for the requirements (i) that it be *simple* (i.e., not reentrant), and (ii) that ψ increase monotonically along ABC and ADC. Requirement (ii) will be relaxed later on.

Figure 1b shows an imagined (q, ψ) scatter diagram obtained by evaluating the scalar quantity q at each available data point on ABCDA and plotting it against the value of ψ at that point. Points A', B', · · · on the circuit correspond to points A, B, · · · on the physical space circuit (Fig. 1a). Here α is the area enclosed by A'B'C'D'A' and β is the area beneath it. The E'F'G'H' is a rectangle enclosing A'B'C'D'A' whose sides are parallel to the q and ψ axes and of length Δq, $\Delta\psi$. Here $\Delta\psi = \psi_+ - \psi_-$ and Δq is the range of values of q on ABCDA.

The net geostrophic flux, F_q, of q out of the area ABCDA is given by

$$F_q = \int_{\mathrm{ABCDA}} q\mathbf{v}_g \cdot \mathbf{n}\,dl = \int_{\mathrm{ADC}} q\frac{\partial\psi}{\partial l}\,dl - \int_{\mathrm{ABC}} q\frac{\partial\psi}{\partial l}\,dl$$

where $\mathbf{n}$ is the outward normal to ABCDA and dl is the line element; see Fig. 1a. Clearly

$$\left.\begin{aligned}\int_{\mathrm{ADC}} q\frac{\partial\psi}{\partial\psi}\,dl &= \int_{\mathrm{A'D'C'}} q\,d\psi = \alpha + \beta \\ \int_{\mathrm{ABC}} q\frac{\partial\psi}{\partial l}\,dl &= \int_{\mathrm{A'B'C'}} q\,d\psi = \beta\end{aligned}\right\}.$$

Hence

$$F_q = \alpha. \qquad (1)$$

The area enclosed by the circuit in (ψ, q) space is equal to the net flux of q (by the geostrophic flow) out of the corresponding area in physical space.

We have assumed that the circuit A′B′C′D′A′ describes the enclosed area in the same sense (anticlockwise) as the circuit ABCDA describes its enclosed area. If this is not so, but A′B′C′D′A′ remains a simple closed curve, then α must be counted as negative, and a net geostrophic flux of q *into* ABCDA is indicated. Further, if A′B′C′D′A′ is reentrant (and thus consists of two or more connected segments), F_q is equal to the area of those segments which are described anticlockwise minus the area of those segments which are described clockwise.

Result (1) also holds for the geostrophic flux of q across any *open* simple curve extending between two points which have the same streamfunction value but which are not coincident. Figure 2a shows such a contour LMN in physical space. The $\psi = \psi_-$ at L and N, and $\psi = \psi_+$ at M; ψ is assumed to increase monotonically along LM and NM. Figure 2b shows a curve L′M′N′ on the (ψ, q) plane which is imagined to correspond to LMN. In this case, in (1), α is equal to the area enclosed by the curve L′M′N′ and the straight line L′N′. If F_q is taken as positive when the flux is from left to right as seen by an observer looking along LMN, then α is to be counted as positive when L′M′N′ is described anticlockwise. Reentrance can clearly be allowed for as above. Note that the values q_L and q_N of q at L and N are not necessarily equal; hence the need, in general, for the line L′N′ to complete definition of the area in (ψ, q) space. However, in regular wave patterns $q_L = q_N$ can be arranged, and hence L′M′N′ closed without the line segment L′N′. Some cases of this type will be examined in section 3.

Result (1) for open curves in physical space may be applied to show that (1) itself holds when ψ varies arbitrarily along the chosen space curves. For example, any section of ABC or ADC (see Fig. 1a) along which ψ does not increase monotonically may be treated as part of a segment of the type LMN (see Fig. 2a); and

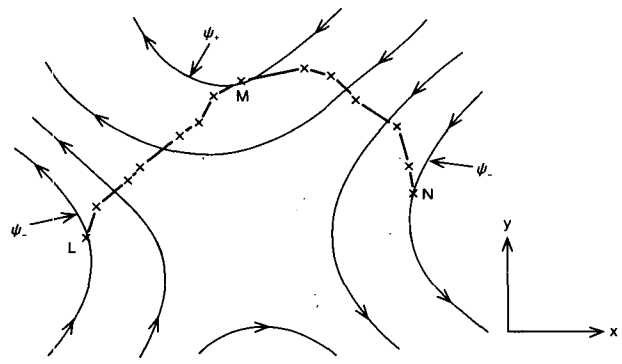

FIG. 2a. An open curve LMN in the (x, y) plane and contours of a geostrophic streamfunction ψ. Note that $\psi = \psi_-$ at both L and N.

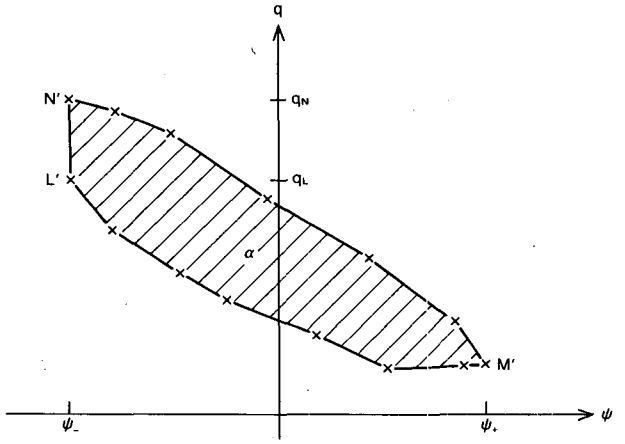

FIG. 2b. The curve L′M′N′ in the (ψ, q) plane which corresponds to the curve LMN in the (x, y) plane. L′N′ is a straight line parallel to the q axis. See text for further details.

it follows that the net geostrophic flux of q out of ABCDA is again equal to the area enclosed on the (q, ψ) diagram.

The same result follows immediately if it is assumed that the mapping $(x, y) \rightarrow (\psi, q)$ is invertible, for then

$$\alpha = \int_{A'B'C'D'A'} d\psi dq = \int_{ABCDA} J(\psi, q) dx dy$$

$$= \int_{ABCDA} q \mathbf{v}_g \cdot \mathbf{n} dl \qquad (2)$$

where $J(\psi, q) = \partial(\psi, q)/\partial(x, y)$ is the Jacobian of the transformation $(\psi, q) \rightarrow (x, y)$. The condition for invertibility is simply that $J(\psi, q)$ should not vanish within ABCDA. However, it is worth noting that no invertibility assumption was necessary in the earlier derivation of (1); we were able to treat reentrant curves in (ψ, q) space, for which 1:1 transformations clearly cannot be defined.

From now on, q will be considered to be the quasi-geostrophic potential vorticity Q. Since α vanishes for any circuit drawn in a flow for which $Q = Q(\psi)$, it is clear that α acts as an indicator of departure from free-mode behavior; but some suitable normalization is required if this departure is to be measured usefully.

Consider first the case of a simple closed curve ABCDA in (x, y) space (see Fig. 1a). Since

$$\alpha = F_Q = \int_{ABCDA} \nabla \cdot (\mathbf{v}_g Q) dx dy$$

$$= \int_{ABCDA} \mathbf{k} \cdot (\nabla\psi \times \nabla Q) dx dy, \qquad (3)$$

it is clear that α depends only on the area enclosed by ABCDA and the mean value of $\mathbf{k} \cdot \nabla\psi \times \nabla Q$ within it. Thus if the area enclosed by ABCDA is held constant, and $\mathbf{k} \cdot \nabla\psi \times \nabla Q$ is effectively constant over

ABCDA, α will not depend on the shape or orientation of ABCDA. A scale estimate for the maximum conceivable value of α is $\Delta\psi\Delta Q$ (see Fig. 1b); this is an estimate, based on (3), of the flux which would be obtained if $\nabla\psi$ and ∇Q were perpendicular to one another throughout ABCDA. Hence

$$I=\frac{\alpha}{\Delta\psi\Delta Q}=\frac{\text{area enclosed on } (Q,\psi) \text{ diagram}}{\text{area of circumscribing rectangle}} \quad (4)$$

is proposed as a measure of the extent of departure from free-mode form over the area ABCDA. However, $\Delta\psi\Delta Q$ is not a least upper bound to F_Q, and [as a consideration of (3) shows] the extent of the overestimate depends on the *orientation* of ABCDA in (x, y) space as well as on its shape. (We are grateful of Prof. B. J. Hoskins for pointing this out to us.) Hence, (4) will give different values of I for space curves which differ only in their orientation. The difficulty may be overcome by considering only circular orbits in physical space, and we are content to adopt this restriction. {Normalization for closed space curves of other shapes may be tackled by noting that $[J(\psi, q)]^{-1}$ is a magnification factor for the transformation $(\psi, q) \rightarrow (x, y)$, but we shall not pursue the problem here.}

In sections 3 and 4 our concern is with scatter diagrams obtained from *open* curves in physical space. For an important class of such open curves, a good measure of the departure from free-mode behavior is the width-to-length ratio of the quasi-elliptical circuit in (ψ, Q) space. This class consists of space curves which approximate to straight lines drawn over one "wavelength" of a streamfunction pattern. As an example, consider the case in which LMN (see Fig. 2a) is a segment of length $2\pi/k$ of the x axis, and ψ and Q vary sinusoidally in x with wavelength $2\pi/k$ and phase difference $\pi - \phi$:

$$\psi=\psi_0 \sin kx; \quad Q=-Q_0 \sin(kx-\phi)$$

(ψ_0 and Q_0 may of course be functions of y). The geostrophic flux of Q across LMN is $\pi\psi_0 Q_0 \sin\phi$. The corresponding (Q, ψ) circuit, when plotted as (Q/Q_0) against (ψ/ψ_0), is an ellipse whose major and minor axes are inclined at 45° to the coordinate axes. It may be regarded as a simple Lissajous' figure. The axis along $Q/Q_0 = -\psi/\psi_0$ has half-length $\sqrt{2}\cos\phi/2$, and the axis along $Q/Q_0 = \psi/\psi_0$ has half-length $\sqrt{2}\sin\phi/2$. The ratio of the minor to major axes (assuming $\phi \leq \pi/2$) is thus $\tan\phi/2$, and the area enclosed, as expected, is $\pi \sin\phi$. The axis ratio $\tan\phi/2$ is a good measure of departure from free-mode form since it vanishes when $\phi = 0$ and is unity when $\phi = \pi/2$.

We have chosen to investigate a simple example, but the suggestion is that the width-to-length ratio, λ, of the loop in (ψ, Q) space is a good general measure of the departure from free-mode form along the corresponding space curve. (It is assumed that ψ and Q are scaled so that their extreme variations along the space curve are nearly equal; or, in other words, that the major axis of the (Q, ψ) diagram is inclined at about 45° to the coordinate axes.)

The published scatter diagrams all include values from all data-or grid points within a stated physical area, rather than only those which lie on a single open or closed curve. Application of the present results to the published work is therefore uncertain. Nevertheless, it is clear that the total area enclosed on any of the published diagrams is an upper bound to the area corresponding to any one chosen circuit in physical space. More important, the width/length ratio of the diagram is an upper bound to the same ratio for any space curve which extends between the lowest and highest streamfunction values. The possibility of the existence of other space curves giving larger width/length ratios cannot be discounted, however.

3. Examples from numerical simulations of rotating annulus flows

To illustrate application of the results derived in section 2 we first examine data from numerical simulations of the steady baroclinic waves which occur in the rotating annulus laboratory system. In the cases to be considered, the fluid is subject to internal heating and is cooled at one or both sidewalls. The internal heating is supplied in the laboratory system by passing an ac current between the sidewalls of the annulus and using a weak electrolyte as the working fluid. The heating is then independent of height and azimuth but varies inversely as the square of the radius. See Hide and Mason (1970), Ukaji (1979) and Read (1984, 1985). The numerical model used for the simulations is a grid-point formulation of the full Navier-Stokes equations for baroclinic flow of an incompressible Boussinesq liquid. Its domain is the annular region bounded by cylindrical sidewalls at $r = a, b$ and rigid horizontal end walls at $z = 0, d$. The grid is stretched in the vertical and radial directions so as to allow adequate resolution of boundary layers without committing a comparable density of points to the interior; the total number of grid-points along each radius and vertical within the domain is sixteen. The separation of the grid in azimuth is uniform and equal to $2\pi/64$. For further details see James et al. (1981), Hignett et al. (1985) and Read (1985).

The quasi-geostrophic potential vorticity Q and geostrophic streamfunction ψ may be calculated at each model grid point at any time from the corresponding pressure (p) and temperature (T) fields by applying the relations

$$\psi=\frac{1}{2\Omega\rho_0}(p-\tilde{p})=\frac{1}{2\Omega\rho_0}p'' \quad (5)$$

$$Q=\frac{1}{2\Omega\rho_0}\left[\nabla^2 p+\frac{4\Omega^2}{\epsilon g}\frac{\partial}{\partial z}\left(\frac{\partial P''}{\partial z}\Big/\frac{d\tilde{T}}{dz}\right)\right]+2\Omega \quad (6)$$

in appropriate finite difference form. In Eqs. (5) and (6), ( ) denotes a variable averaged over the entire horizontal area of the fluid (at a given height) and ( )″ the departure from this average; ∇^2 is the horizontal Laplacian operator; g is the acceleration due to gravity; Ω is the rotation rate of the frame of the annulus; and ρ_0 and ϵ are the mean density and thermal expansion coefficient of the fluid.

Figures 3b and 3c show fields of ψ and $\hat{Q} = Q - 2\Omega$ at height $0.87d$ as calculated from the steady wave fields obtained in a simulation with internal heating, cooling at the inner sidewall and an insulating outer sidewall (see Read 1984, Case D). This steady flow had a regular four-wave structure. The values of ψ and $\hat{Q}$ were not calculated at grid points which lay within the highly ageostrophic boundary layers adjacent to the sidewalls. The general similarity in form of the ψ and $\hat{Q}$ fields shown in Fig. 3b and 3c is borne out by the conventional scatter diagram of the ψ and $\hat{Q}$ values within one wavelength of the steady wave pattern (Fig. 3a). All of the points are found within a narrow strip passing close to the origin in the $(\psi, \hat{Q})$ plane; the correlation coefficient is -0.96. Such a close anticorrelation suggests that the flow is close to the idealized "free mode" form $Q = Q(\psi)$ referred to in section 1.

In Fig. 3a all the points which correspond to grid points lying on the circle $r = a + 0.33(b - a)$ have been joined up in order of azimuthal position. The simple curve thus formed is a narrow loop whose enclosed area is equal to the radial potential vorticity flux by the geostrophic flow over one wavelength of the steady wave (see section 2). The significance of this flux may be assessed from the width-to-length ratio λ of the loop; we find $\lambda \approx 0.05$ for the particular loop outlined in Fig. 3a. The quantity λ expresses the smallness of the departure of the flow from free-mode form and allows comparison with other systems (or other regions of the same system).

A more complicated example is shown in Fig. 4a. Data for this example were taken from height $0.755d$ in another steady baroclinic wave simulation with (height-dependent) internal heating, and cooling at both sidewalls (see Read 1986). The anti-correlation between ψ and Q is clearly much less marked than in the previous example: the correlation coefficient is -0.62. This is borne out by Fig. 4b and c, which show the ψ and $Q - 2\Omega$ fields containing the grid-point values plotted in Fig. 4a. Evidently the flow in this case departs significantly from free-mode form. In Fig. 4a all the points corresponding to $r = a + 0.33(b - a)$ in physical space over one wavelength of the flow have been joined up in order of azimuthal position. The loop so described is re-entrant, and its two sections each have a width-to-length ratio of about 0.25. This value confirms the considerable departure of the flow from free-mode form. However, the radial potential vorticity flux by

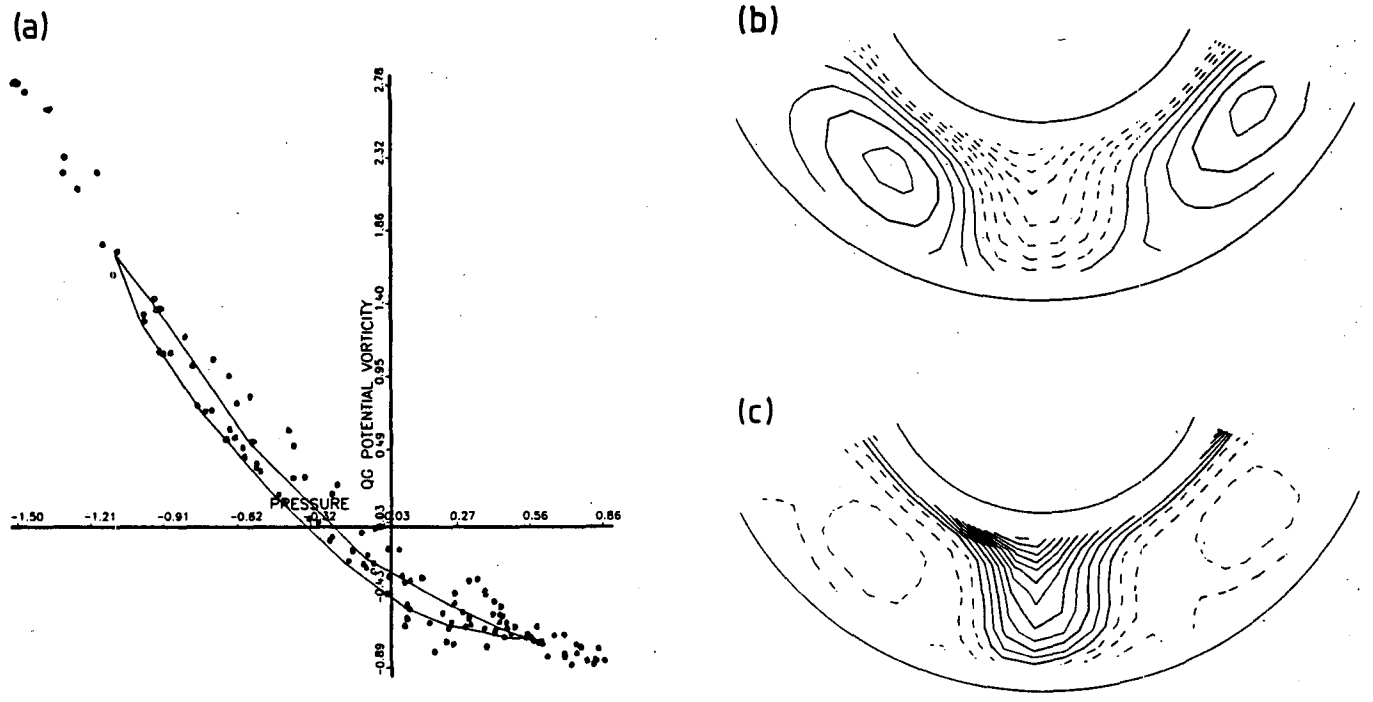

FIG. 3. (a). Scatter diagram of the grid-point values of streamfunction and relative potential vorticity $Q - 2\Omega$ used to plot the maps shown in (b) and (c). (b) Maps of the streamfunction (b) and relative potential vorticity (c) at height $0.87\times$ annulus depth in a steady wave simulation with internal heating applied. Cooling takes place via the inner sidewall; outer sidewall is thermally insulating. Potential vorticity is measured in units of s^{-1} (contour interval 0.25); streamfunction is plotted as $2\Omega\psi$, in units of $cm^2\ s^{-2}$ (contour interval 0.2). Negative contours dashed.

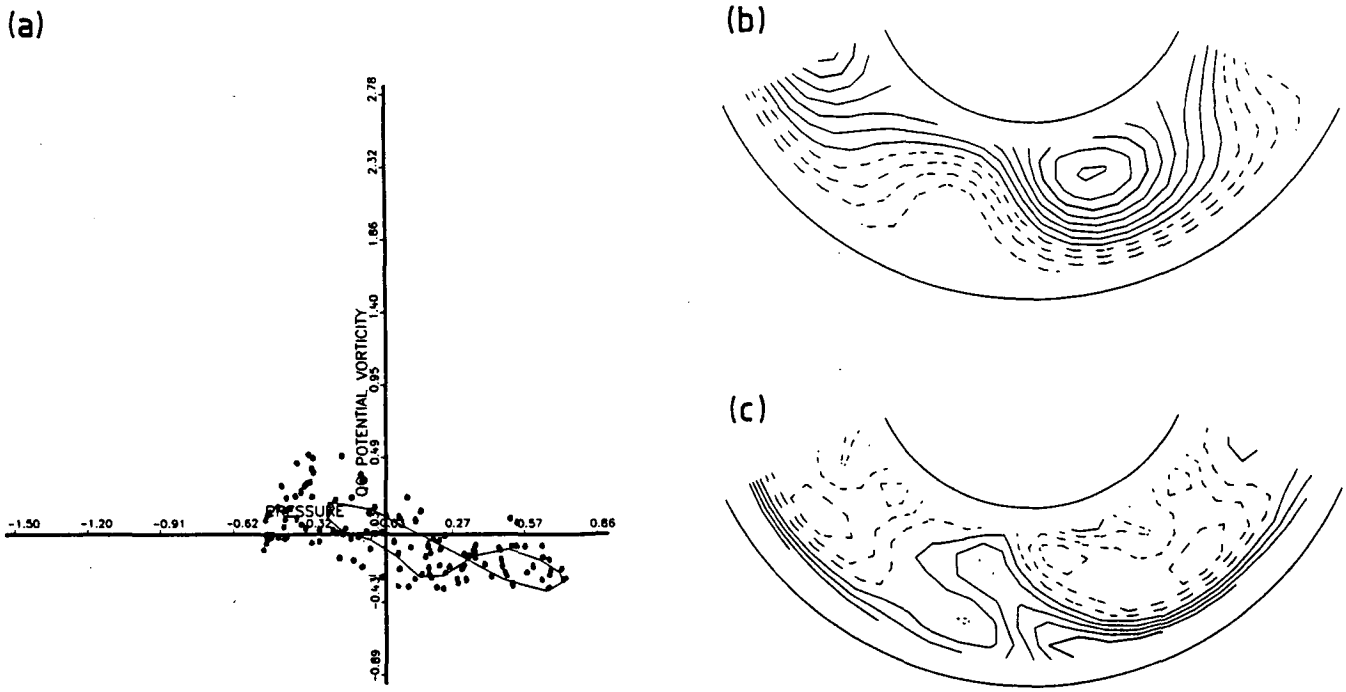

FIG. 4. As for Fig. 3 but for a case in which cooling takes place via both sidewalls and the internal heating is height dependent; data obtained from height 0.755× annulus depth in numerical simulation. Contour intervals: 0.10 for both $(Q - 2\Omega)$ and $2\Omega\psi$.

the geostrophic flow is equal to the difference in the areas of the two sections of the loop, since each contributes oppositely to $\oint Q d\psi$. The net radial potential vorticity flux in this case is therefore much less than the conventional diagram 4a would suggest: only when loops corresponding to concentric circles in physical space are traced out does the smallness of the flux become apparent. (The near-cancellation in the present case reflects the fact that the potential vorticity flux due to the first azimuthal harmonic of the dominant Fourier component of the flow at this level is in the opposite sense to that due to the dominant component itself).

Since the meridional flux of potential vorticity is an important measure of the interaction between eddy and zonal mean flow (e.g., see Edmon et al., 1980), the example shown in Fig. 4 demonstrates how a naive interpretation of a conventional (ψ, Q) scatter diagram could give a misleading impression of the dynamics of the flow. Greater insight may be achieved by relating the points on the scatter diagram to orbits in physical space.

4. Examples from numerical simulations of the general ocean circulation

Although the steady-state or time-averaged fields in a fluid system may approach a free mode state, forcing and dissipative processes are present in real flows and are conceptually and physically important. In this section we illustrate how (Q, ψ) scatter diagrams for time-mean fields can be used to deduce information about the forcing and dissipative processes, as well as about potential vorticity fluxes. We examine fields obtained using the eddy-resolving ocean circulation model developed by W. Holland. The simulations are part of a study of general circulations driven by combined wind stress and thermodynamic forcing. There are three constant-density layers in the vertical, with 200 × 200 grid points in the horizontal, simulating a 4000 km × 4000 km × 5 km square ocean basin with rigid vertical sidewalls.

We shall look at the $Q - \psi$ signature of an ocean driven by steady winds, and then show the effect of adding successively stronger thermal forcing.

Figure 5a shows the time-mean streamfunction for the middle layer of a typical wind-driven circulation. There are two counterrotating gyres separated by an intense eastward flowing jet, the model realization of the separated Gulf Stream or Kuroshio. Along the western boundary lie boundary currents which reconnect the meridional circulation occurring in the interior.

The wind-driven circulation shrinks in scale as one proceeds downward from the sea surface. At this intermediate depth the fluid is remote from the direct effect of the wind (the Ekman pumping acts only on the upper layer of this quasi-geostrophic model), and there is a tendency for Q to be conserved along streamlines. Eddy form drag occurs, however, which is the

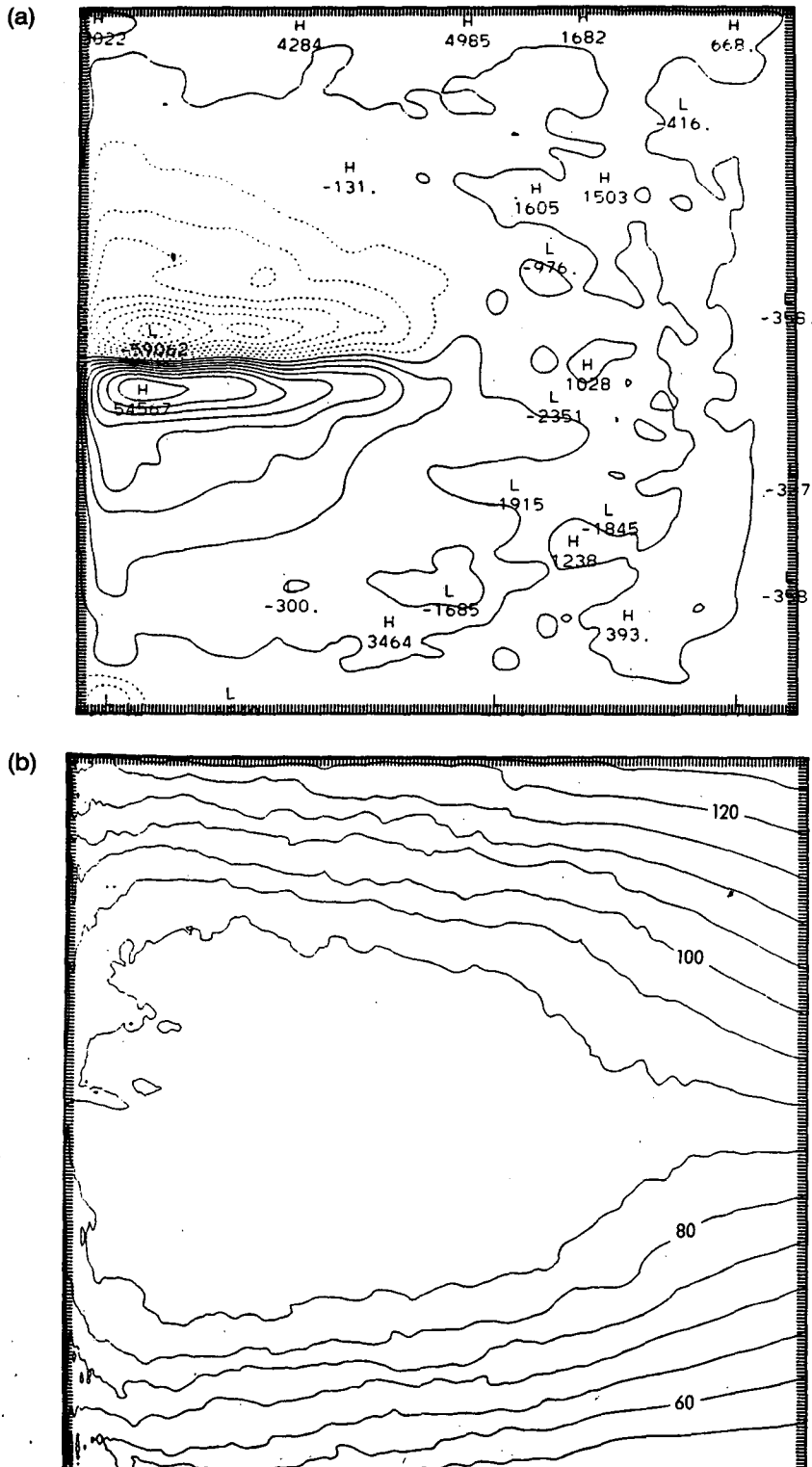

FIG. 5. (a) Mean streamfunction and (b) potential vorticity for the middle of the three constant density layers of the quasi-geostrophic model. Driving is by steady winds with no thermal forcing. The pair of wind gyres has shrunk in size, compared with their form nearer the sea surface. The potential vorticity is nearly uniform across much of the region of circulation. Units of ψ are $m^2\ s^{-1}$, of Q are $m^{-1}\ s^{-1}$. Contour intervals: 7×10^3 (ψ), 5×10^{-6} (Q). Negative ψ contours dashed. (c) Scatter diagram of mean potential vorticity (ordinate) versus mean streamfunction (abscissa) for the flow shown in (a) and (b). (d) $Q - \psi$ scatter plots at selected latitudes in the basin (from single cuts across (a) and (b). The labels 40, 60 and 80 refer to gridpoints respectively 800, 1200 and 1600 km north of the southern boundary (the basin is 4000 km across).

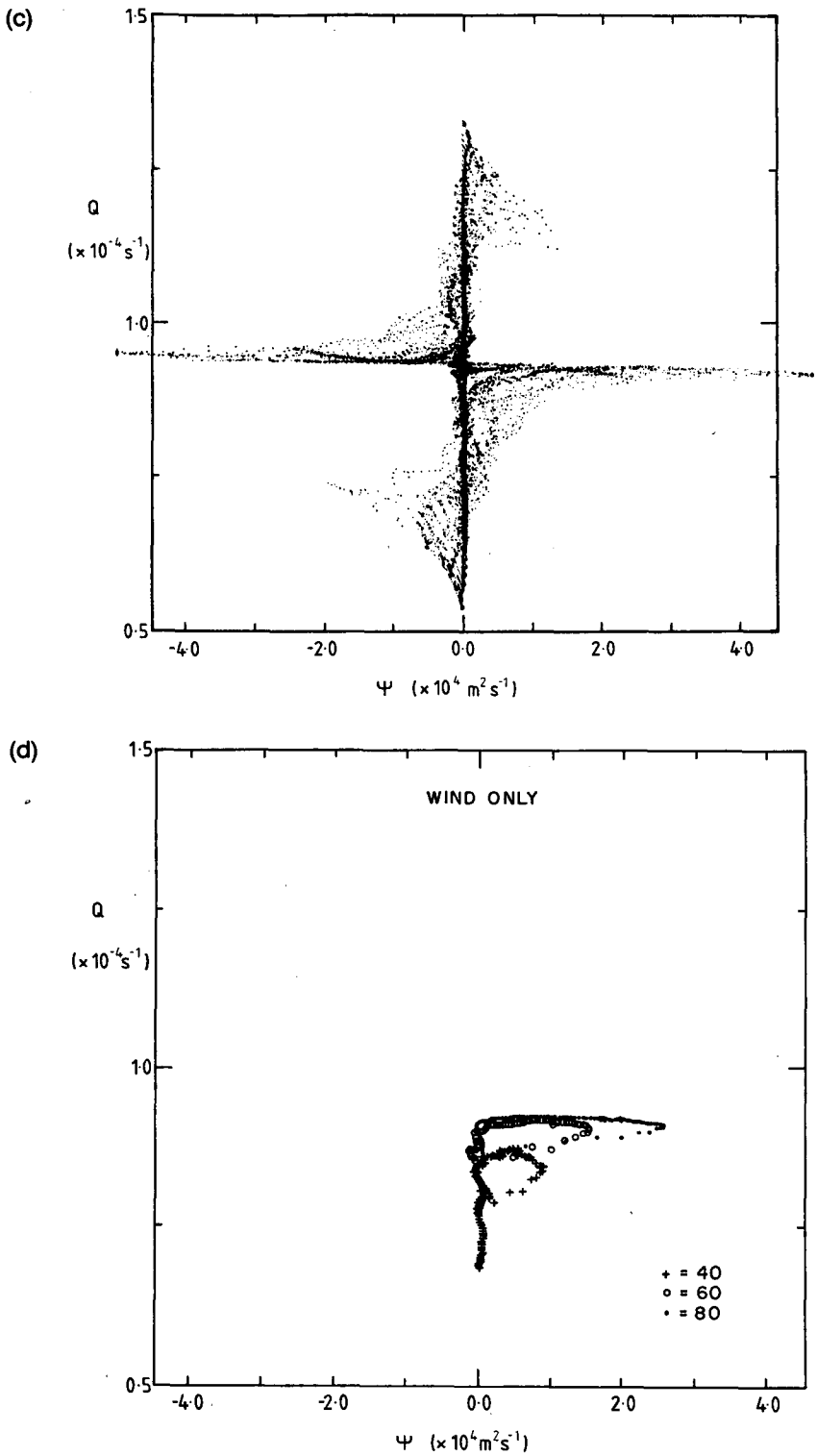

FIG. 5. (*Continued*)

driving agent carrying the wind-gyre momentum downward, and this causes the $Q - \psi$ relation to be imperfect (see Holland and Rhines, 1980). The mean potential vorticity for the same layer, Fig. 5b, shows the ironic fashion in which the potential vorticity conservation occurs. Gradients of Q are expelled by eddy

potential vorticity flux, leaving a homogeneous interior distribution (Rhines and Young, 1982, 1983). The corresponding global scatter diagram, Fig. 5c, shows the form of a cross; to a first approximation the degenerate $Q - \psi$ relation is one in which either Q vanishes where ψ is nonzero, or conversely.

Regions of uniform Q may be regarded as one of several "building blocks" of the general circulation. They are characteristic of "isovortically forced" domains; that is, regions driven from above or below by motion of isopycnal surfaces which do not alter the potential vorticity (the potential vorticity equation having no forcing term, while the energy and momentum equations do so). A theory for this process is provided by extension of the Prandtl-Batchelor theorem to geophysical, turbulent flows (Rhines and Young, 1982).

Figure 5d shows the contributions from three selected latitudes (see caption) to the global scatter plot (Fig. 5c). The horizontal arms correspond to the Q-homogenized wind-driven gyre (the southernmost plot showing the gradient at the edge of the gyre). The vertical arms correspond to the resting fluid outside the gyre, and the widely spaced points to the boundary currents. In relation to their lengths, all three circuits enclose considerable areas, and the southernmost loop (+ =40) has a width-to-length ratio of about unity. This evidently reflects the contribution of the boundary currents to the north–south potential vorticity flux, and indicates that the free-mode picture is not appropriate at all longitudes.

When driving stresses or buoyancy sources exert themselves directly on the fluid interior the signatures are rather different. In Fig. 6c we see the effect on the mean scatter diagram of a weak thermal forcing in the form of heat sources and sinks in the eastern parts of the basin. The vertical arm of the cross is broadened as a range of ψ occurs, corresponding to weak, closed thermal gyres. The spatial maps of circulation and potential vorticity (Figs. 6a, b) show the weak thermal gyres lying to the east of the wind gyres, in the region of the buoyancy forcing (heavy dashed contours). If we look at the contributions to this global scatter plot from single latitudes, Fig. 6d, we again see disconnected figures, with "arms" corresponding to the wind gyre (horizontal segment), the thermal gyre (inclined arm at left) and the western boundary current (sparse points making up right arm). The nonvanishing enclosed area indicates that the net north–south flux of potential vorticity by the mean circulation does not vanish, and again suggests the importance of the boundary currents (in which dissipative processes are significant).

When the thermal driving is increased in strength by a factor of 5 (with the winds held the same), the potential vorticity signatures of the stronger thermal gyres are different again (Fig. 7). Now the thermal driving is stronger than the effect of the wind in this middle layer (though the two driving effects are comparable nearer the sea surface). The thermal gyres encroach on the wind gyre, and great islands of potential vorticity form. This is by necessity: the presence of internal sources and sinks of sufficient strength requires persistent mean gradients of Q. The relevant diagnostic is given by the following argument (see Rhines and Young, 1982, 1983; Pierrehumbert and Malguzzi, 1984; Marshall and Nurser, 1986).

Suppose we have a potential vorticity source of strength S within the fluid, and suppose that the eddy transport of potential vorticity is approximated by a down-gradient diffusion with constant diffusivity K. If the Peclet number of the flow, VL/K (based upon velocity scale V, horizontal length scale L), is sufficiently large, then the (time averaged) potential vorticity equation

$$J(\psi, Q) = S + K\nabla^2 Q \tag{7}$$

has an approximate solution

$$Q = Q(\psi). \tag{8}$$

The exact integral of (7) over the area enclosed by a mean streamline gives

$$-K\int \nabla Q \cdot \mathbf{n} dl = \int S dx dy.$$

Using equation (8) this may be written as

$$-\frac{dQ}{d\psi} = \frac{\int S dx dy}{K\int \mathbf{v}\cdot d\mathbf{l}} \tag{9}$$

which determines diagnostically the functional relation between Q and ψ. The difficulty in practice is that the circulation in the denominator must be known. In some cases (9) can be used to solve for the circulation completely.

The relation (9) has homogenization as a special case, for $S = 0$. But we see the inevitable gradient of Q that must occur when S is nonzero, in order to carry away diffusively the potential vorticity being created by S.

The sign of $dQ/d\psi$ is significant. Notice that, except in the extreme case of homogenization (Fig. 5), all of the scatter plots shown in this section lean downward to the right. This negative sign of $dQ/d\psi$, to the extent that there is a systematic correlation, is appropriate for flows in which the potential vorticity due to some driving agent S has the same sense as the *relative* vorticity that the twisting due to S would produce. That is, a cyclonic twisting force produces cyclonic potential vorticity, and if the relative vorticity is also cyclonic in sense, then this lean is inevitable. Counterexamples can be found, in which more remote forcing (say, an anticyclonic wind stress above) causes large positive Q to be correlated with large positive ψ (for example through the presence of a strong barotropic mode). [Dr. J. C. Marshall has drawn to our attention cases in which

$dQ/d\psi > 0$ in the lowest layer of an ocean model when dissipation occurs via bottom friction and there is no heating (see also Niiler, 1966)].

Arnol'd's stability theorem (e.g., see Blumen 1968) shows that in free flows with $Q = Q(\psi)$ a negative slope, $dQ/d\psi < 0$, in some region of the flow is necessary for infinitesimal perturbations to grow. We have already noted that negative slopes occur almost universally in the simulations here. Indeed, mesoscale eddies are active in transporting potential vorticity, particularly in the sense of a form drag of one layer upon another. Here, the thermal driving creates counterrotating circulations lying one above another, and these resist one another by eddy interfacial drag, tending to reduce the transport of each gyre. The eddies occur from baroclinic instability particularly where $\partial Q/\partial y$ changes sign in the vertical, in the east-central region of the basin.

The scatter plots in Figs. 7c, d again show separate arms—corresponding respectively to the two wind gyres (the horizontal arms), the two principal thermal gyres (in the first and third quadrants) and to two minor thermal gyres lying near the northern and southern boundaries of the basin (second and fourth quadrants of the scatter plot). The near collapse of the points onto a single curve in the main thermal gyres indicates that, despite the forcing, the flow is acting like a free Q-conserving steady flow. Subsets taken at single values of y (Fig. 7d) show rather small areas enclosed by the points, and hence the north–south potential vorticity flux by the mean geostrophic flow is small. Consistently, the width-to-length ratios, and hence the departure from free-mode form are small. All this does not mean, however, that eddy effects are negligible. Indeed, the transports of the counterrotating thermal gyres (lying one above another) are less than predicted by linear or steady nonlinear theory. Eddies act through inviscid form drag as a strong vertical momentum diffusion. For the forced region, the forcing S is nearly balanced by dissipation across a latitude line, leaving near conservation of Q following mean streamlines. In fact, as the above analysis shows, S must be exactly balanced by dissipative or eddy transport of Q, if one averages over an area enclosed by a mean streamline. But the scatter plots succinctly show that the mean circulation is not carrying potential vorticity across latitude circles, at least in this region of the model ocean.

Arguments similar to the above can also be applied to simulated steady annulus waves such as those discussed in section 3 (see Figs. 3 and 4). For these cases, the terms in (7) representing departures from perfect conservation of Q correspond to the effects of molecular diffusion (viscosity and thermal conduction) and internal heating (Read, 1985, 1986). Suppose that ν and κ are the kinematic viscosity and thermal diffusivity of the model fluid. Horizontal diffusion produces a term $\nu\nabla^2 Q$ in the potential vorticity balance—essentially as in (8). The source S then represents the effects of internal diabatic heating (cf. Pedlosky 1979), the vertical derivatives of the diffusion terms and a further term arising from the effects of thermal conduction (present only if $\kappa \neq \nu$). Thus

$$S = 2\Omega\frac{\partial}{\partial z}[H/N^2] + D_v + (\kappa - \nu)4\Omega^2\frac{\partial}{\partial z}[\nabla^2(\partial\psi/\partial z)/N^2] \tag{10}$$

where H is the internal heat source in the thermodynamic equation, N is the buoyancy frequency, and D_v represents the effects of vertical diffusion. For regions of the fluid in which the quasi-geostrophic approximation is valid (i.e., well outside the Ekman and sidewall boundary layers; for example, see Read, 1985) vertical gradients are small compared with those in the horizontal. In the absence of internal heating, (9) suggests therefore that $dQ/d\psi$ will also be small and that near-homogenization of Q will occur if $\kappa = \nu$. For almost all working fluids used in rotating annulus experiments, $\nu > \kappa$, however, and the situation is complicated by the presence of the third term in (10). In cases where the flow is driven by internal heating, (10) is generally dominated by the first term on the right side in regions outside thermal boundary layers (see Read, 1986), and S is positively correlated with potential vorticity. For the example in Fig. 3, for which $\nu \approx 9\kappa$, the scatter diagram is characterized by $dQ/d\psi$ being negative and nearly uniform across the annulus (except towards the sidewalls), indicating a further positive correlation between S (due to internal heating) and the *relative* vorticity at the vertical level considered—in a way analogous to the thermally-driven component of the ocean circulation illustrated in Fig. 7.

5. Conclusion

Dynamical insight into the nature of complex geophysical flows, such as those presented here, is vastly aided by analysis of large-scale maps of mean circulation and potential vorticity. The (Q, ψ) scatter diagrams offer a simple yet effective means of interpreting these maps, giving information on the mean transport of potential vorticity, on the degree of departure from free-mode form, and on the dissipative and forcing processes acting on the flow.

The relations between this diagnostic view and basic questions of conservation and stability are of great interest. Conservation theorems for the quantity

$$\text{wave energy} + [\text{wave enstrophy}/(dQ/d\psi)],$$

which subsume Arnol'd's theorem, have recently been discussed (e.g., see Andrews, 1983; McIntyre and Shepherd, 1986). It is significant that simulations of geophysical circulations so often develop approximate parallelism of mean streamlines and mean potential vorticity contours, despite significant eddy (or viscous) transports of Q. The suggestion is that consideration

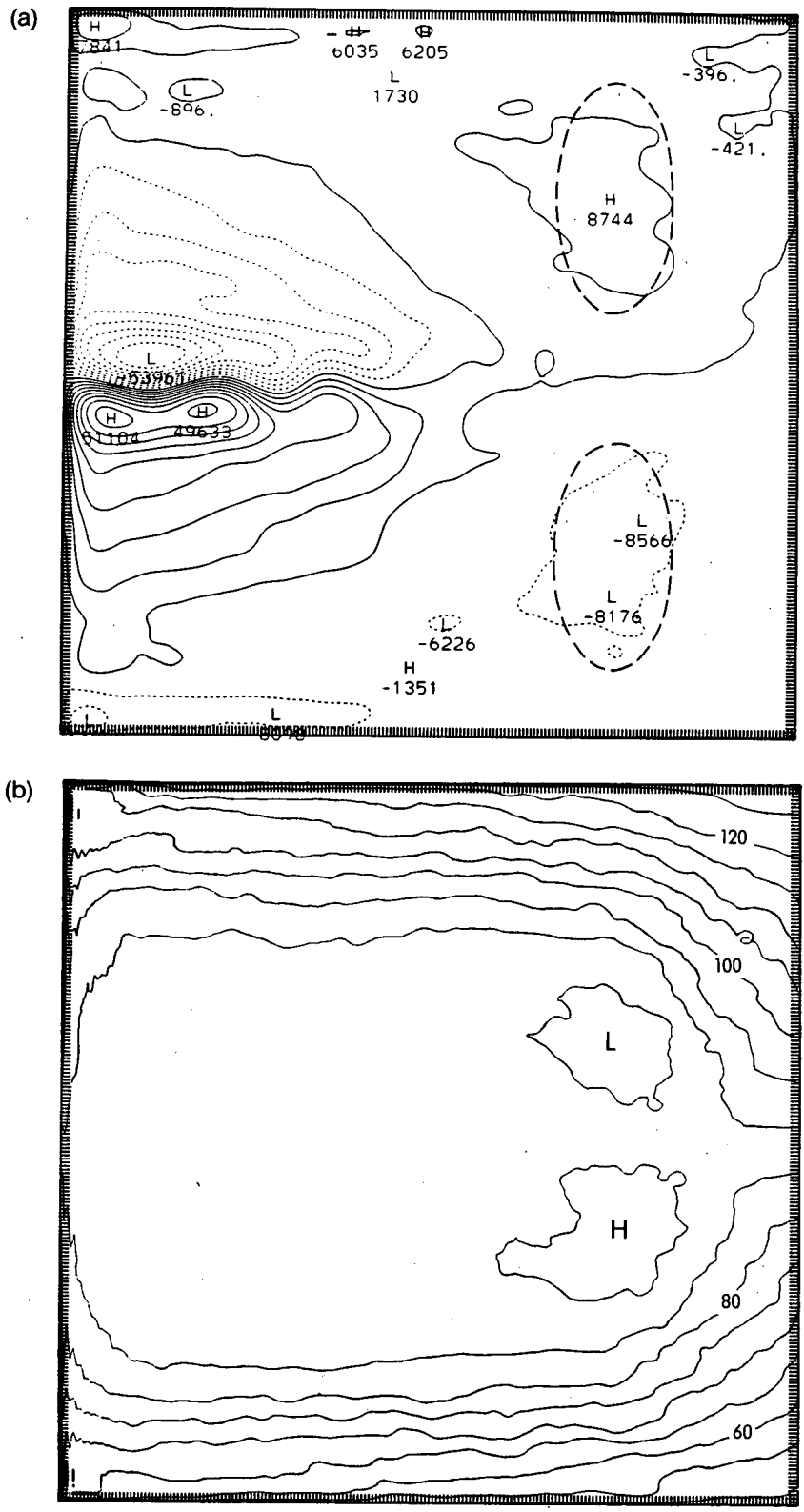

FIG. 6. (a) ψ and (b) Q for a case with wind-driving combined with *weak* thermal forcing. The region of thermal forcing is shown by heavy dashed curves. Contour intervals: 6×10^3 (ψ), 5×10^{-6} (Q). (c) Global scatter plot of Q vs ψ for the flow in (a) and (b). (d) $Q - \psi$ diagrams for three latitudes [as in (d)]. The weak buoyancy forcing expands the region of closed circulation, and distinctly tilts the $Q - \psi$ plot in regions previously at rest. The thermal- and wind-driven circulations, though meshed together in physical space, are clearly distinct in this diagram.

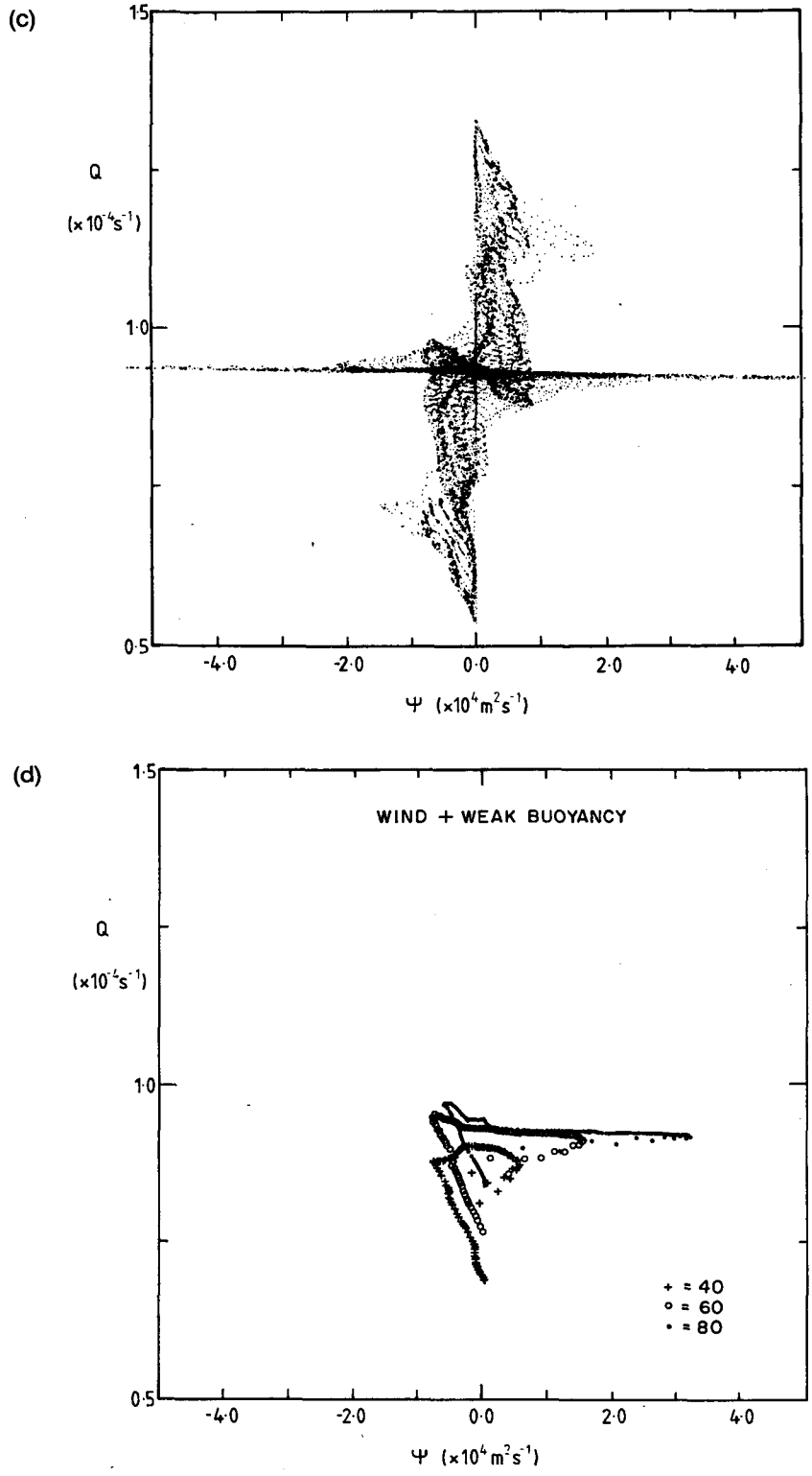

FIG. 6. (*Continued*)

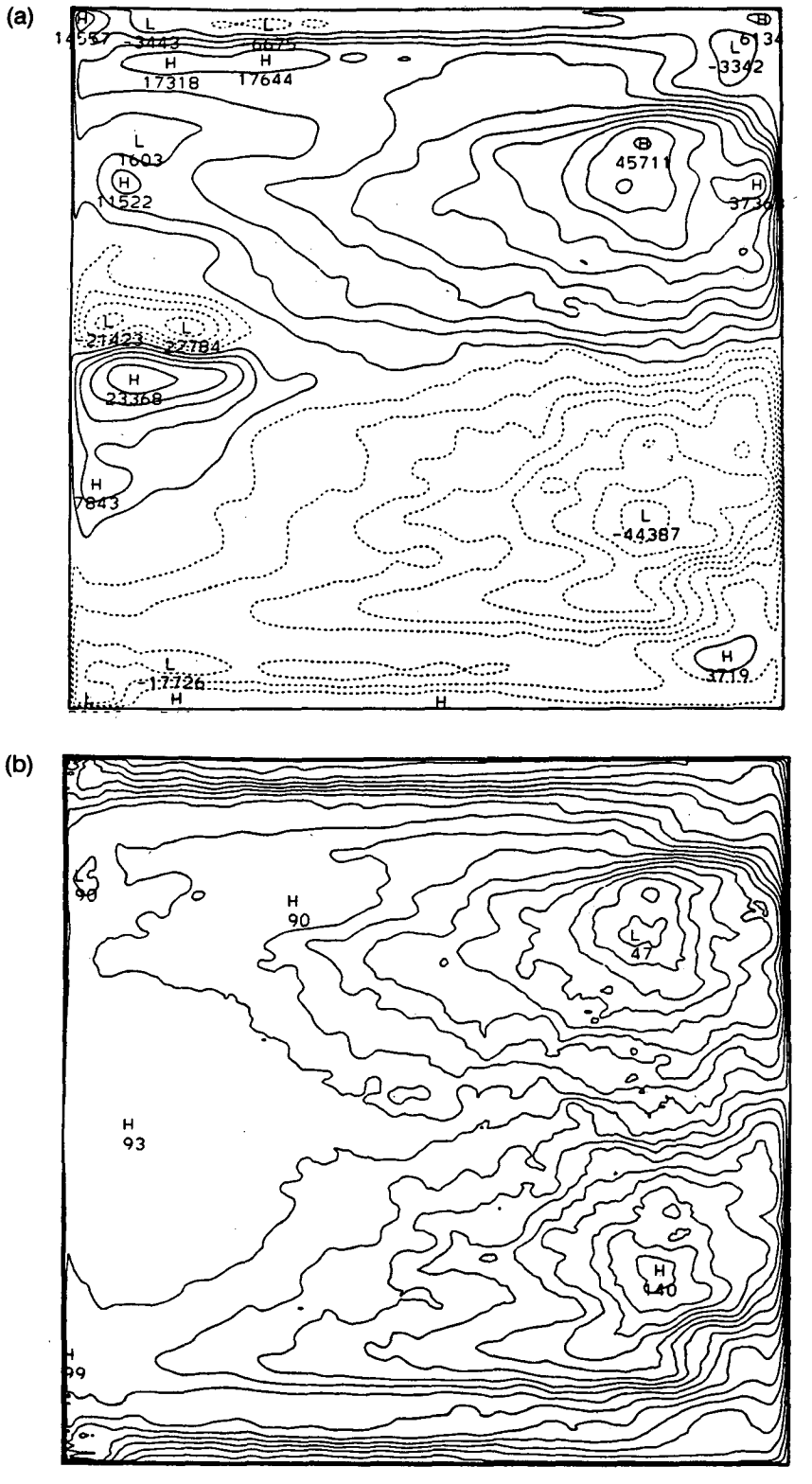

FIG. 7. As in Fig. 6 but with wind driving combined with *strong* buoyancy driving (5 times the strength of that in Fig. 6). Now the "thermal" gyres are very strong, and the scatter diagram [(c) and (d)] tends to collapse close to a single curve. This suggests that the gyres have some "free inertial" characteristics, even though the eddy transport and forcing terms are individually large. The grid has been stretched at both meridional boundaries. The boundary currents are well resolved and show up as widely spaced points dipping below the main sequence. Contour interval for ψ: 5×10^3 and for Q: 5×10^{-6}.

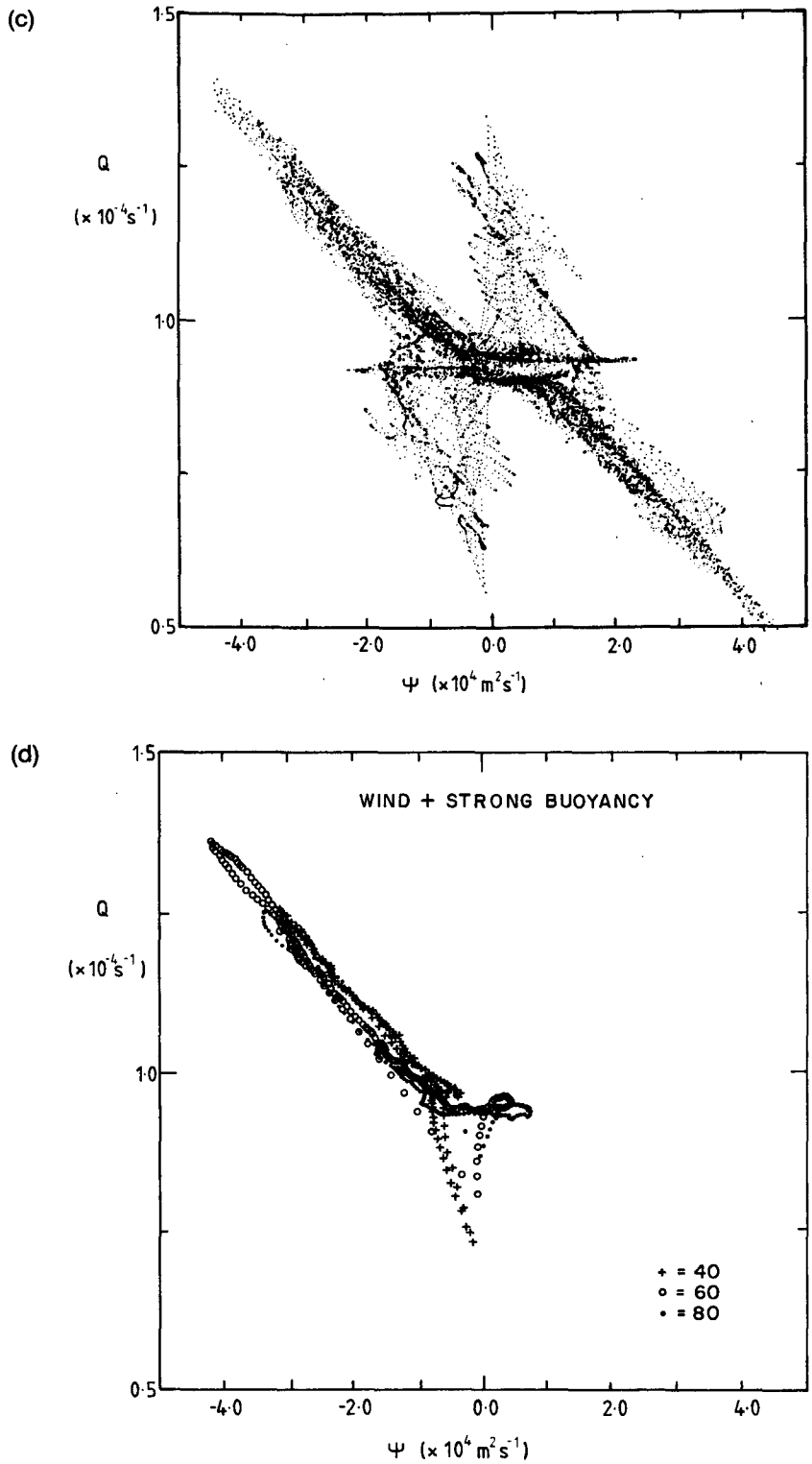

FIG. 7. (*Continued*)

of idealized conservative flows may be more relevant to nature than once suspected.

In this paper attention has been limited to scatter diagrams based on quasi-geostrophic potential vorticity Q and the geostrophic streamfunction ψ. Dr. D. G. Andrews has drawn to our attention, however, that the

hydrostatic primitive equations for steady, free flow imply the Jacobian identities $J(\chi, E) = 0$, $J(\chi, B) = 0$. Here E is Ertel's potential vorticity, B is the Bernoulli energy function, χ is a streamfunction and the Jacobians are defined with respect to horizontal differentiation on isentropic surfaces. Furthermore, $E = \partial B/\partial\chi$. A similar development is possible also for nonhydrostatic flow. In either case the problem of identifying free-modes analytically appears to be intractable; but the vanishing Jacobians suggest a straightforward method of data analysis whereby approach to free-mode form in real or simulated flow would be gauged from scatter diagrams of E or B plotted against χ. The relations derived here in sections 2 and 4 in the context of quasi-geostrophic dynamics are evidently applicable to the more general cases with only slight modification.

Acknowledgments. We are grateful to Prof. B. J. Hoskins for his helpful criticism of an earlier version of this paper, and also to Drs. D. G. Andrews, J. D. Gibbons, J. C. Marshall and G. J. Shutts for useful comment and discussion.

REFERENCES

Andrews, D. G., 1983: A conservation law for small-amplitude quasi-geostrophic disturbances on a zonally asymmetric basic flow. *J. Atmos. Sci.*, **40,** 85–90.

Blumen, W., 1968: On the stability of quasi-geostrophic flow. *J. Atmos. Sci.*, **25,** 929–931.

Bretherton, F. P., and D. B. Haidvogel, 1976: Two-dimensional turbulence above topography. *J. Fluid Mech.*, **78,** 129–154.

Derome, J., 1984: On quasi-geostrophic finite amplitude disturbances forced by topography and diabatic heating. *Tellus,* **36,** 313–319.

Edmon, H. J., B. J. Hoskins and M. E. McIntyre, 1980: Eliassen-Palm cross sections for the troposphere. *J. Atmos. Sci.*, **37,** 2600–2616.

Flierl, G. R., V. D. Larichev, J. C. McWilliams and G. M. Reznik, 1980: The dynamics of baroclinic and barotropic solitary eddies. *Dyn. Atmos. and Oceans,* **5,** 1–41.

Hide, R., and P. J. Mason, 1970: Baroclinic waves in a rotating fluid subject to internal heating. *Phil. Trans. Roy. Soc. London,* **A268,** 201–232.

Hignett, P., A. A. White, R. D. Carter, W. D. N. Jackson and R. M. Small, 1985: A comparison of laboratory measurements and numerical simulations of baroclinic wave flows in a rotating cylindrical annulus. *Quart. J. Roy. Meteor. Soc.*, **111,** 131–154.

Holland, W. R., and P. B. Rhines, 1980: An example of eddy-induced circulation. *J. Phys. Oceanogr.*, **10,** 1010–1031.

Illari, L., and J. C. Marshall, 1983: On the interpretation of eddy fluxes during a blocking episode. *J. Atmos. Sci.*, **40,** 2232–2242.

James, I. N., P. R. Jonas and L. Farnell, 1981: A combined laboratory and numerical study of fully developed steady baroclinic waves in a cylindrical annulus. *Quart. J. Roy. Meteor. Soc.*, **107,** 51–78.

Kuo, H.-L., 1959: Finite amplitude three-dimensional harmonic waves on the spherical earth. *J. Meteor.*, **16,** 524–534.

McIntyre, M. E., and T. G. Shepherd, 1987: An exact conservation theorem for finite amplitude disturbances to nonparallel shear flows, with remarks on Hamiltonian structure and on Arnol'd's stability theorems. *J. Fluid. Mech.*, submitted.

McWilliams, J. C., 1983: Interactions of isolated vortices. *Geophys. Astrophys. Fluid Dyn.*, **24,** 1–22.

——, 1984: The emergence of isolated coherent vortices in turbulent flow. *J. Fluid Mech.*, **146,** 21–43.

——, and N. J. Zabusky, 1982: Interaction of isolated vortices. I: Modons colliding with modons. *Geophys. Astrophys. Fluid Dyn.*, **19,** 207–227.

Marshall, J. C., and G. Nurser, 1986: Steady, free circulation in a stratified quasi-geostrophic ocean. *J. Phys. Oceanogr.*, (in press).

Mitchell, H. L., and J. Derome, 1983: Blocking-like solutions of the potential vorticity equations: their stability at equilibrium and growth at resonance. *J. Atmos. Sci.*, **40,** 2522–2536.

Niiler, P. P., 1966: On the theory of wind-driven ocean circulation. *Deep-Sea Res.*, **13,** 597–606.

Pedlosky, J., 1979: *Geophysical Fluid Dynamics.* New York, Springer-Verlag, 624 pp.

Pierrehumbert, R. T., and P. Malaguzzi, 1984: Forced coherent structures and local multiple equilibria in a barotropic atmosphere. *J. Atmos. Sci.*, **41,** 246–257.

Read, P. L., 1984: Finite amplitude, neutral baroclinic waves and mean flows in an internally heated rotating fluid: numerical and analytical models of stable eddies in the laboratory. Meteorological Office, Met 0 21 Intern. Rep. IR/84/5 [available from Meteorological Office Library, London Road, Bracknell, Berkshire, RG12 2SZ, U.K.].

——, 1985: Finite amplitude, neutral baroclinic eddies and mean flows in an internally heated rotating fluid: 1. Numerical simulations and quasi-geostrophic 'free modes'. *Dyn. Atmos. and Oceans,* **9,** 135–207.

——, 1987: Finite amplitude, neutral baroclinic eddies and mean flows in an internally-heated rotating fluid: 2. Effects of spatially-varying N^2. Submitted to *Dyn. Atmos. Oceans.*

Rhines, P. B., 1977: The dynamics of unsteady currents. *The Sea,* Vol. 6, ed. E. N. Goldberg and co-Editors, Wiley-Interscience, 189–318.

Rhines, P. B., and W. R. Young, 1982: Homogenization of potential vorticity in planetary gyres. *J. Fluid Mech.*, **122,** 347–367.

——, and ——, 1983: How rapidly is a passive scalar mixed within closed streamlines? *J. Fluid. Mech.*, **133,** 133–145.

Shutts, G. J., 1983: The propagation of eddies in diffluent jetstreams: eddy vorticity forcing of blocking flow fields. *Quart. J. R. Met. Soc.*, **109,** 737–761.

Stern, M. E., 1975: Minimal properties of planetary eddies. *J. Mar. Res.*, **33,** 1–13.

Tribbia, J. J., 1984: Modons in spherical geometry. *Geophys. Astrophys. Fluid Dynamics,* **30,** 131–168.

Ukaji, K., 1979: Thermal and dynamical structures of convective motions in a rotating annulus subject to internal heating. *J. Met. Soc. Japan,* **57,** 532–547.

White, A. A., 1986: Finite amplitude, steady Rossby waves and mean flows—analytical illustrations of the Charney-Drazin non-acceleration theorem. *Quart. J. R. Met. Soc.*, **112,** 749–773.